Author Manuscript

Author Manuscript

Author Manuscript

Author Manuscript

HHS Public Access

Author manuscript

Magn Reson Med. Author manuscript; available in PMC 2019 June 01.

Published in final edited form as:

Magn Reson Med. 2018 June ; 79(6): 2902–2911. doi:10.1002/mrm.26949.

Reduced Acoustic Noise in Diffusion Tensor Imaging on a Compact MRI System

Ek T. Tan, Ph.D.[1], **Christopher J. Hardy, Ph.D.**[1], **Yunhong Shu, Ph.D.**[2], **Myung-Ho In, Ph.D.**[2], **Arnaud Guidon, Ph.D.**[3], **John Huston III, M.D.**[2], **Matt A. Bernstein, Ph.D.**[2,†], and **Thomas K.F. Foo, Ph.D.**[1,†]

[1]GE Global Research, Niskayuna, NY, USA

[2]Department of Radiology, Mayo Clinic, Rochester, MN, USA

[3]GE Healthcare, Boston, MA, USA

Abstract

Purpose—To investigate the feasibility of substantially reducing acoustic noise, while performing diffusion tensor imaging (DTI) on a compact 3T (C3T) MRI scanner equipped with a 42-cm inner diameter asymmetric gradient.

Methods—A-weighted acoustic measurements were made using 10 mT/m-amplitude sinusoidal waveforms, corresponding to echo-planar imaging (EPI) echo spacing of 0.25–5.0 ms, on a conventional, whole-body 3T MRI and on the C3T. Acoustic measurements of DTI with trapezoidal EPI waveforms then were made at peak gradient performance on the C3T (80 mT/m amplitude, 700 T/m/s slew rate) and at derated performance (33 mT/m, 10–50 T/m/s) for acoustic noise reduction. DTI was acquired in two different phantoms and in seven human subjects, with and without gradient-derating corresponding to multi- and single-shot acquisitions, respectively.

Results—Sinusoidal waveforms on the C3T were quieter by 8.5–15.6 dBA on average as compared to the whole-body MRI. The derated multi-shot DTI acquisition noise level was only 8.7 dBA (at 13 T/m/s slew rate) above ambient, and was quieter than non-derated, single-shot DTI by 22.3 dBA; the scan time was however, almost quadrupled. While derating resulted in negligible diffusivity differences in the phantoms, small biases in diffusivity measurements were observed in human subjects (ADC = +9.3±8.8%, FA = +3.2±11.2%, RD = +9.4±16.8%, PD = +10.3±8.4%).

Conclusion—The feasibility of achieving reduced acoustic noise levels with whole-brain DTI on the C3T MRI was demonstrated.

Keywords

Silent MRI; diffusion tensor imaging; compact 3T; head-only scanner

Correspondence: Ek T. Tan, Ph.D., GE Global Research, One Research Circle, Niskayuna, NY 12309, USA, Phone: 518-387-7075, Fax: 518-387-6923, ek.tan@ge.com.

[†]These authors contributed equally.

Author Manuscript Author Manuscript Author Manuscript Author Manuscript

INTRODUCTION

Acoustic noise in MRI impacts patient and operator safety of MRI, and is one of the four main categories considered by the U.S. Food and Drug Administration (FDA) when considering the significant risk of clinical MR systems. Acoustic noise results from Lorentz forces between the main magnetic field and conductors carrying time-varying electric current in the gradient system. This interaction causes vibrations that generate sound pressure waves [1–2] that could be harmful if not controlled or mitigated. For *in vivo* human MRI, regulatory bodies such as the FDA mandate acoustic noise limits for non-significant risk operation (A-weighted root mean square sound pressure levels less than or equal to 99 dBA with hearing protection in place, and less than or equal to 140 dB peak, unweighted sound pressure level). Even with hearing protection in place, acoustic noise is a major source of patient discomfort that increases with field strength [3], affecting both adult and pediatric populations especially at 3T and above [4]. Furthermore, acoustic noise from the gradients impedes communication between the patient and the scan operator [5]. Acoustic noise is potentially a major confound in some brain imaging, and in particular has been shown to influence results of functional MRI studies [6–7]. In addition, quiet or silent MRI has distinct advantages when studying pediatric populations, especially for assessing brain function or brain development.

Brain MRI frequently employs echo-planar imaging (EPI) readout, which can benefit from acoustic noise reduction. EPI typically employs a train of trapezoidal readouts with short echo spacing. Data are acquired at high readout bandwidth (±125–250 kHz), and EPI readouts tend to have higher acoustic noise than their counterparts in standard imaging [8–9]. Fast gradient switching and high gradient amplitudes, characteristic of EPI, are primary reasons for the high level of acoustic noise in functional MRI (fMRI), and also in diffusion imaging of the brain.

Several countermeasures have been proposed to reduce acoustic noise. In addition to the use of hearing protection and noise-cancellation earphones, software-based noise reduction approaches have been proposed. Zero-echo-time pulse sequences employing three-dimensional radial k-space trajectories and high-bandwidth [10–11] or frequency-swept [12] RF excitation employ gently-stepped, rather than rapidly switched gradients, and so are virtually silent. However, these sequences intrinsically yield proton-density contrast [11] and generally require relatively fast RF switching. Another strategy is to replace trapezoidal gradient waveforms during MRI with sinusoidal waveforms [13–16]. Those ‘silent’ approaches effectively attenuate higher-frequency components of the acoustic noise spectrum. They also apply a degree of gradient derating that result in longer gradient rise time (i.e., reduced slew rate) in conjunction with lower readout bandwidth, which result in reduced readout gradient amplitudes, in turn reducing the Lorentz forces. Robust noise reduction has been demonstrated at 1.5–4T MRI with gradient-echo [13–14, 17], fast spin echo/turbo spin echo [13–14, 18], and even multi-echo, gradient-echo readouts [19]. Applying the same techniques in EPI, however, has proved to be more challenging, because it is louder to begin with, and because derating inevitably further reduces the phase-encoding bandwidth, aggravating the severe image distortion [20]. A notable attempt to reduce acoustic noise in diffusion-weighted EPI utilized a combination of sinusoidal waveforms,

Author Manuscript Author Manuscript Author Manuscript Author Manuscript

gradient derating, and readout-segmented multi-shot EPI. While this achieved a promising 19.1–21.7 dBA noise reduction in whole-body MRI scanners at both 1.5T and 3T [21], when tested in a clinical imaging protocol at 1.5T, it only achieved a more modest 10.3 dBA reduction [22]. Another attempt at reducing acoustic noise in gradient-echo EPI for fMRI combined constant phase-encoding with sinusoidal EPI with a reported 20 dB (unweighted) noise reduction, using specific frequency troughs in the frequency response function in order to demonstrate this extent of improvement [23].

While many gradient hardware-based acoustic reduction methods have also been proposed, only a few methods have been implemented in conventional, clinical MRI scanners, including mechanical isolation, acoustic foam, acoustic barriers, and force-balancing [24–25]. Other methods include utilizing torque-balancing [26], vacuum enclosures [27], and active feedback for vibration control [28]. Interestingly, smaller gradient coil inserts, for brain-imaging in particular [29–30], generally have quite different acoustic characteristics [31] than whole-body gradient coils used in conventional MRI. To first approximation, the harmonic oscillation frequency is inversely proportional to the square-root of mass; therefore, smaller gradient coils with smaller mass may have a higher range of resonating frequencies. Smaller gradient coils typically also have greater efficiency or gain, i.e., less electric current is needed to generate equivalent gradient amplitude [32].

Work on a recent head-only, gradient coil with 26-cm field-of-view, force- and torque-balanced design [33–34] verified that peripheral nerve stimulation (PNS) thresholds higher than that in whole-body MRI can be achieved [34–35]. The gradient coil employed asymmetric design on the transverse axes (i.e., physical X and Y). The higher PNS thresholds allow for imaging humans *in vivo* at much higher peak gradient amplitude (80 mT/m) and slew rate (700 T/m/s) simultaneously, reducing EPI echo-spacing by as much as two-fold [36]. This gradient was installed in a low-cryogen, compact 3T (C3T) magnet, and produced acoustic measurements at its peak performance that were within regulatory guidelines, comparable to that of a whole-body 3T MRI system operating at much lower performance [37]. The acoustic performance of the C3T at derated gradient performance has not yet been reported.

In this work, we present initial results investigating the feasibility of using the C3T scanner to reduce acoustic noise in diffusion-weighted EPI acquisitions. We hypothesize that diffusion tensor imaging (DTI) will produce significantly lower sound levels on the C3T than on a whole-body scanner at equivalent gradient amplitude and slew-rate, both for gradient-derated and non-derated imaging. We apply derating to the DTI acquisition to bring about further acoustic noise reduction, which will, however, result in undesirable increased image distortion. We hypothesize that the incorporation of multi-shot DTI with derating will nevertheless yield substantially lower sound levels without introducing significant bias in quantitative DTI diffusivity measurements (ADC, FA, etc.).

Author Manuscript Author Manuscript Author Manuscript Author Manuscript

METHODS

Acoustic measurements with sinusoidal waveforms

Acoustic noise measurements on the C3T were made, using a conventional, whole-body, 3T scanner as a reference. To analyze the fundamental frequencies of the trapezoidal EPI waveforms that would be used later in imaging, sinusoidal gradient waveforms at 18 discrete frequencies were played for ten-second durations at 10 mT/m amplitude. These frequencies ranged from 100 to 2000 Hz with increments of 100–200 Hz, corresponding to EPI echo-spacing (ESP) of 250–5000 μs (0.5–10.0 ms periodicity). Identical gradient waveforms were generated on the conventional whole-body 3T MRI scanner with gradients capable of 50 mT/m peak amplitude and 200 T/m/s slew rate (MR750, GE Healthcare, Waukesha WI, USA) and on the head-only C3T MRI scanner (80 mT/m, 700 T/m/s). Each physical gradient axis (X for right-left, Y for anterior-posterior, and Z for superior-inferior direction) was pulsed separately.

Acoustic measurements were made using a Model G4, Type 2250 handheld analyzer and Type 4189 microphone (Brüel & Kjær, Nærum, Denmark). The A-weighted, equivalent continuous sound level was recorded in decibels (dBA), resetting the measurement immediately before each pulse sequence or waveform and taking the median between two measurements made immediately upon completion of each pulse sequence or waveform. The ambient noise level was also recorded before and after each measurement session.

Acoustic measurements of DTI with trapezoidal EPI readout

An axial DTI pulse sequence was prescribed with a 24 cm-field-of-view, 2.5 mm-isotropic spatial resolution, one T2-weighted (b-value=0 s/mm^2) acquisition, ten diffusion directions (b-value=1,000 s/mm^2), fat-saturation, and single-spin-echo trapezoidal EPI readout with ramp-sampling in the physical X (left-right) direction. Without derating, the peak gradient performance of each MRI scanner was applied, abiding by first-level controlled mode PNS limits. On the C3T, the PNS limit was set to that of the most PNS-restrictive axis (X, or left-right) [34]. With derating, the peak gradient amplitude on the C3T was additionally limited to 33 mT/m and the EPI gradient slew rate was also reduced and varied in eight steps between 10 and 50 T/m/s. The TR was fixed at six seconds, maximizing the number of allowable slices for each run based on the minimum allowable TE for each slew rate setting. The ESP for each slew rate was recorded. Acoustic measurements were performed after the calibration “reference” scan and the first TR, so that all the gradient waveforms including phase-encoding blips and diffusion-encoding gradients contributed to the acoustic noise measurement.

Phantom acquisition on compact 3T MRI

To evaluate robustness to SNR and measurement repeatability, the DTI data were first acquired using a 16-cm diameter, spherical MR spectroscopy phantom (GE Healthcare, Waukesha WI, USA). The phantom temperature was equilibrated to ambient temperature in the scanner room (20 °C) overnight prior to each scan. Imaging was performed using two different receive-only brain coils – an 8-channel phased-array coil (Invivo Diagnostics, FL, USA) and a 32-channel phased-array coil (Nova Medical, Inc., MA, USA). The acquisition

Author Manuscript Author Manuscript Author Manuscript Author Manuscript

on the 32-channel coil was repeated on a separate day at the same ambient temperature. Square 7.1–7.9 cm regions-of-interest (ROIs) were drawn on three central slices for analysis.

To evaluate the effects on quantitative diffusivity values, another acquisition was performed with a Quantitative Imaging Biomarkers Alliance (QIBA) diffusion phantom (High Precision Device, Inc., Boulder CO, USA). This 19.4-cm diameter phantom [38] was filled and temperature-controlled at 0±0.2 °C with de-ionized ice-water bath during image acquisition. It contained thirteen 3-cm diameter cylindrical vials with varying concentrations of polyvinylpyrrolidone (PVP) [39] as modifiers of diffusivity. The vials were arranged in two concentric rings with PVP concentration ranging from 0–50% in 10% increments. Comparisons were made against referenced diffusivity values [40] previously obtained with DTI. The 8-channel coil was used, as the 32-channel coil was too small to accommodate the phantom. The phantom was placed at the center of the coil for axial acquisition of the cross-section of the vials. Quadrilateral ROIs of area 45–144 mm^2 were drawn on the cross-section images of each vial and on three central slice locations for analysis. The variation in ROI area was to avoid highly distorted regions due to the small size of the vials and associated EPI susceptibility effects.

DTI acquisitions were performed on the C3T with both standard (i.e., non-derated), single-shot DTI and derated, multi-shot DTI. A slew rate of 13 T/m/s (ESP = 2.0 ms) was used in the derated, multi-shot acquisition, corresponding to a sound pressure level of 8.7 dBA above ambient. TR/TE was kept fixed in both acquisitions at 6000/83.3 ms, matching the TR and minimum TE for the derated, multi-shot DTI. For the standard, non-derated single-shot DTI, a slew rate of 700 T/m/s was applied, resulting in an ESP of 332 μs. Parallel imaging (ASSET, acceleration=2) was applied to the standard DTI to reduce image distortion. For the derated DTI, multi-shot acquisition (four shots) was used to reduce image distortion; this yielded a maximum of 45 slices for 11.25-cm slice coverage. The scan time (including a TR for relaxation equilibrium) was 1.2 minutes and 4.5 minutes, respectively for the standard and the four-shot derated DTI. Fig. 1 shows a composite of the gradient waveforms of the standard and derated DTI on the readout-axis, showing the effects of derating on both the diffusion and EPI waveforms.

An iterative image reconstruction scheme was developed on MATLAB (Mathworks, Natick MA, USA), similar to [41] to account for phase inconsistencies [42] that typically occur with multi-shot DTI *in vivo*. Standard images reconstructed on the scanner were also used for the phantom multi-shot EPI.

Human subject acquisition on compact 3T MRI

Seven human subjects with no known neurological disease (age=31.9±10.3 years, 5F/2M) were recruited and scanned on the C3T in accordance with an IRB-approved protocol, after providing written, informed consent. All subjects were scanned with the same DTI protocol as the phantom studies, but only with the 32-channel coil. As before, the number of slices per TR was maximized to give 11.25 cm axial slice coverage. The iteratively-reconstructed images were used for DTI processing and analysis. Eddy-current-induced distortion was corrected using the real-time field-adjustment feature [43] on the scanner. Correction for susceptibility-induced distortion was not applied.

Author Manuscript Author Manuscript Author Manuscript Author Manuscript

All acquisitions on the C3T employed real-time gradient pre-emphasis [44] and B_0 compensation [45] to account for additional concomitant field terms due to the asymmetric gradient design of the transverse (physical X- and Y-) gradients on the C3T. For DTI processing, an independently-validated tenth- and even-ordered spherical harmonics-derived gradient field map [45] was used to correct for gradient nonlinearity of both spatial distortion and diffusivity-encoding [46–47].

Standard DTI metrics – apparent diffusion coefficient (ADC), fractional anisotropy (FA), radial diffusivity (RD) and parallel diffusivity (PD) were computed. Six ROIs were drawn for analysis in the following anatomical regions – corpus callosum frontal/occipital (CCF/CCO), the primary motor regions corresponding to the feet (left and right), and in the left and right cerebral peduncles in the brain stem (BS) that encompass the corticospinal tracts. Statistical analysis was performed by paired t-test ($P<0.05$ considered as statistically significant), with normalized percentage differences between derated and non-derated DTI denoted as ΔADC, ΔFA, ΔRD and ΔPD. In the phantom study, ΔFA was not normalized to avoid division by zero because the phantoms used were isotropic (expected FA=0).

RESULTS

Acoustic measurements with sinusoidal waveforms

Without accounting for differences in ambient noise, the sinusoidal waveforms at 10 mT/m amplitude on the C3T MRI scanner were quieter than on the whole-body scanner by 12.2±12.0 dBA, 15.6±11.9 dBA, and 8.5±7.2 dBA on the X-, Y- and Z-axes respectively. The ambient noise was louder on the C3T system by 2.8 dBA, which increases these differences when considered. Fig. 2 shows the acoustic noise level above ambient for both scanners with all three gradient axes as a function of the corresponding ESP. With all axes, the C3T was quieter than the whole-body MRI; in particular, on the X-axis (the primary axis used for EPI in brain imaging), a 27–36 dBA advantage was observed on the C3T in the range of ESP=500–625 μs. When the ESP was increased to over >2000 μs, the noise was <1 dBA over ambient on the C3T.

Acoustic measurements of DTI with trapezoidal EPI readout

Fig. 3a shows the effects of derating the gradient slew rate on ESP. A very short ESP of 332 μs was obtained with the maximum slew rate of the C3T (700 T/m/s). Reducing the slew rate to the 10–50 T/m/s range increased ESP to the range of 1.0–2.3 ms. Fig. 3b shows the resulting acoustic noise measurements, where the sound pressure level over ambient was reduced at increased ESP, down to <10 dBA at ESP≥2 ms. Therefore, for phantom and *in vivo* imaging, the slew rate was derated to 13 T/m/s, resulting in ESP=2.0 ms the acoustic noise was 8.7 dBA above ambient. As compared to non-derated DTI, the noise level was reduced by 22.3 dBA in the derated DTI.

Phantom acquisition on compact 3T MRI

Fig. 4 shows a summary of the results on the MRS phantom. For every permutation of receiver coil, day and method for image reconstruction (standard or iterative), there was no statistically-significant difference in the diffusivity metrics between the derated multi-shot

Author Manuscript Author Manuscript Author Manuscript Author Manuscript

and non-derated single-shot DTI. The mean differences in the metrics were small, with ΔADC=−1.0% to 0.0%, ΔFA = +0.008 to 0.024, ΔRD=−1.8% to 0.6%, ΔPD=−0.1% to 1.8%. With iterative reconstruction, these differences were slightly closer to zero, but this effect was not statistically significant. These differences were in the range of test-retest reproducibility; the day-one minus day-two ADC on the 32-channel coil were −0.6±0.1% for non-derated, −1.0±1.3% for non-derated with standard reconstruction, and −1.4±0.8% for non-derated with iterative reconstruction. For FA, the reproducibility numbers were: −0.002±0.006, −0.013±0.012, and −0.005±0.003. For RD, the corresponding values were: −0.5±0.1%, −0.3±0.7%, and −1.1±0.6%. For PD, these were −0.7±0.2%, −2.2±2.3%, and −1.9±1.0%.

Fig. 5 summarizes the results on the QIBA diffusion phantom. The ADC, RD and PD measurements with standard image reconstruction were about identical between derated and non-derated DTI; the constant of proportionality (and Pearson's correlation coefficient) was found to be 1.03 (r>0.99) for ADC, 1.00 (r>0.99) for RD and 1.09 (r>0.99) for PD. With iterative reconstruction on the derated DTI, the proportionality results were slightly closer to unity at 1.02 (r>0.99) for ADC, 1.00 (r>0.99) for RD and 1.06 (r>0.99) for PD. The FA measurements in the majority of the compartments were under <0.2, except for 5/13 of the vials which had the lowest diffusivity values and the highest PVP concentration (40–50%). The corresponding proportionality (and correlation) for FA obtained with standard reconstruction of derated DTI vs that from standard reconstruction of non-derated DTI was 1.8 (r=0.93), and that vs iterative reconstruction of non-derated DTI was 2.2 (r=0.97).

Table 1 summarizes results of the measured ADC values as compared against the published reference [40]. Both the non-derated ADC and derated ADC with iterative reconstruction did not have any vial with a statistically-significant difference against the reference value. For derated ADC with standard reconstruction, small but statistically-significant positive biases (11–28%) were observed in two of the vials with the highest PVP concentration and lowest diffusivities.

Human subject acquisition on compact 3T MRI

Fig. 6 shows representative diffusivity maps (trace, ADC and FA) obtained from the derated DTI scan from one subject (M, 39 years). The brain major brain structures can be well visualized, including the corpus callosum, motor cortex and brain stem regions that were selected for analysis.

Fig. 7 compares diffusivity maps (ADC, FA, RD and PD) between the derated and standard, non-derated axial DTI in another subject (F, 23 years), reformatted in the sagittal orientation. Visually, the intensity and colorized orientation of the major brain structures appeared similar. However, increased EPI distortion in the phase-encoding direction was discernable in the derated DTI images. As compared to standard single-shot DTI with ESP=332 μs (parallel imaging factor of 2), the multi-shot derated DTI with ESP=2 ms (four shots) had increased effective echo spacing by approximately three-fold, corresponding to theoretically increased distortion by also approximately three-fold.

Author Manuscript Author Manuscript Author Manuscript Author Manuscript

Fig. 8 summarizes the comparison of the diffusivity analysis. In the CCF, CCO and BS regions, ADC, RD and PD were mostly higher in the derated multi-shot DTI than in the non-derated single-shot DTI. However, these results were statistically significant only in the CCF (ΔADC=+11.2% with P=0.026 and ΔPD=+10.0% with P=0.022) and in the right BS (ΔADC=+15.4% with P<0.001, ΔRD=+18.4% with P<0.001, and ΔPD=+14.5% with P=0.021). The ΔFA was not statistically different from zero in any region.

DISCUSSION

We believe that these initial results demonstrate the feasibility of substantially reducing acoustic noise in whole-brain DTI on the compact 3T (C3T) MRI scanner. The C3T was first found to be significantly quieter (by 8.5–15.6 dBA on average) than the whole-body scanner at EPI-relevant frequencies. Relative to non-derated DTI on the C3T, a noise reduction of 22.3 dBA (8.7 dBA above ambient) was achieved with the derated DTI without the use of sinusoidal waveforms, albeit at the cost of quadrupled scan time and at about tripled image distortion despite using multi-shot EPI. In isotropic phantoms, the diffusivity metrics were repeatable and comparable to published reference values. However, there were some small differences in some diffusivity metrics between non-derated and derated DTI that were found in human subject studies.

With the exception of FA, excellent agreement in ADC, RD and PD was observed between standard and derated DTI in the phantom studies. It is likely that the discrepancy of FA results in the phantom was due to the fairly isotropic phantom medium, which could be more susceptible to shot-to-shot phase variation and bias from the image reconstruction technique used. Several reasons may explain the discrepancies observed in human subject study measurements of ADC, RD, PD but not in the phantom studies. With derating, the diffusion pulse widths were increased by approximately 2.5 times, given that the diffusion-encoding gradient amplitude were reduced (33 mT/m vs. 80 mT/m). The derated DTI also used multi-shot EPI and iterative reconstruction for phase recovery, which seemed to improve the quantitative accuracy of diffusivity values; standard DTI was single-shot and did not require iterative reconstruction. We speculate that that incomplete phase recovery in multi-shot DTI could result in signal cancellation that would artificially increase the computed diffusivity. The derated DTI also had lower readout bandwidth allowed by the lower readout gradient amplitude than that of the non-derated DTI, which in theory would result in about 2.3 times higher SNR. Although the SNR in the 2.5 mm-isotropic acquisition was deemed adequate, it is known that lower SNR can artificially reduce measured diffusivity (in non-derated DTI) [49]. In addition, there would be differences in ROI selection due to residual eddy-current-induced distortion in the derated DTI. While distortion was higher by about three-fold in the derated DTI (after considering the number of shots and acceleration factor of parallel imaging), the C3T scanner typically has only half the image distortion as compared to whole-body scanners [36]. Therefore, as compared to non-derated DTI on a whole-body scanner, the derated DTI on the C3T has only approximately 1.5-fold worse distortion. In addition, standard methods to correct for the EPI-related geometric distortion were not applied, as the primary focus of this work was to demonstrate the feasibility of achieving substantial acoustic noise level reduction with the prototype C3T scanner. However, correction of gradient-nonlinearity in diffusivity [46] had been found to be necessary on the

Author Manuscript Author Manuscript Author Manuscript Author Manuscript

C3T [50] in order for diffusivity values to be compared quantitatively as was done in this work.

Although the application of derated EPI resulted in increased EPI distortion as compared to that achievable with whole-body MRI, the images may still be usable in clinical practice. In this work, we did not evaluate the clinical utility of the quieter, derated DTI sequence, which would be one goal of our future work. To bring about further reduction in image distortion, it is possible to increase the number of EPI shots. However, there will be increased image reconstruction challenges due to the shot-to-shot variation of phase in diffusion-encoded images [42]. In addition, a higher shot factor would increase the contribution of noise due to increased area of phase-encoding waveforms. A more detailed comparison of noise contributions of frequency-encoding vs. that of phase-encoding waveforms at varying shot factors would be needed.

Although substantial sound pressure level reduction down to 8.7 dBA above ambient was achieved in this work, there would be at least three other ways to improve further on the acoustic performance. The TR and TE on the standard DTI were matched to that of the derated DTI, that is they were longer than the minimum possible TR/TE. Therefore, a TR/TE-optimized DTI on the C3T would potentially be louder than that in this study; so the 22.3 dBA improvement demonstrated here is possibly a slight under-estimation of the potential acoustic noise improvement from derating. It is also possible to lengthen the TR of the derated DTI to further reduce the mean sound pressure level. However, increasing the TR will only have an incremental effect on the mean sound pressure level, and will have negligible effect on peak sound pressure level. In this work, the number of slices per TR was maximized in order to maximize the packing of gradient waveforms that is done in many clinical protocols. For these reasons, the A-weighted equivalent continuous (root mean square) sound level reported in this work was a reasonable depiction of the sound experienced by a human subject. Another way to potentially further reduce noise would be to replace trapezoidal EPI with sinusoidal EPI [21–22], as well as using constant phase-encoding waveforms and measurement of the frequency response function to identify specific frequency troughs [23]. Doing so is likely to reduce noise in EPI either with or without derating. The differences in ambient noise between the two systems (the C3T ambient was louder by 2.8 dBA) could be attributed to differences in the magnet, cold-head and shroud of the C3T system for which the ambient acoustic noise considerations were not of primary importance in its design.

In addition, since the C3T system is capable of a higher peak gradient amplitude of 80 mT/m, the TE of the derated sequence may be shortened by allowing for the peak gradient amplitude to be applied in the diffusion waveforms while derating the EPI waveforms. This relies on diffusion waveforms having a smaller acoustic contribution than EPI, which had been observed in the literature [21]. This TE reduction is expected to be more significant for larger b-values.

The 42-cm inner diameter asymmetrical gradient design on the C3T system has higher PNS thresholds in brain imaging [34] and provides superior gradient performance to whole-body gradient designs for applications such as DTI and fMRI [36]. Reduced acoustic noise

Author Manuscript Author Manuscript Author Manuscript Author Manuscript

especially at EPI-relevant ESPs provides an added advantage to the C3T – improving patient comfort and safety, as well as avoiding possible physiologic confounding effects in neuroscience studies. In preliminary tests comparing acoustic sound pressure levels at the same maximum gradient amplitude and slew rate as in a whole-body 3T system (33 mT/m and 120 T/m/s), the asymmetric head-gradient was observed to have between 3–9 dBA lower acoustic sound pressure levels in EPI, fast gradient echo, and steady-state free-precession pulse sequences. It is likely that other 'silent' or 'quiet' pulse sequences will also be quieter on the C3T than on whole-body 3T systems when operating at the same gradient performance. Alternatively, the C3T may be able to provide equivalent noise performance as whole-body scanners but at higher gradient strengths and slew rate that can improve key parameters such as TR, TE, ESP and scan time. The force- and torque-balanced design of the C3T's head-only gradient may also help to reduce lower-frequency vibrations common in diffusion-weighted imaging; vibration measurements are planned as part of future work.

In conclusion, the feasibility of acoustic noise reduction on diffusion-weighted EPI was demonstrated on the head-only compact 3T MRI scanner. That, together with its high gradient performance gradients and its light weight, low-cryogen magnet that simplifies siting, makes this scanner a suitable platform for advancing the state-of-the-art for neuroimaging.

Acknowledgments

Grant support: NIH R01EB010065

References

1. Hedeen RA, Edelstein WA. Characterization and prediction of gradient acoustic noise in MR imagers. Magn Reson Med. 1997; 37(1):7–10. [PubMed: 8978626]
2. Mansfield P, Glover PM, Beaumont J. Sound generation in gradient coil structures for MRI. Magn Reson Med. 1998; 39(4):539–50. [PubMed: 9543415]
3. Price DL, De Wilde JP, Papadaki AM, Curran JS, Kitney RI. Investigation of acoustic noise on 15 MRI scanners from 0.2 T to 3 T. J Magn Reson Imaging. 2001; 13(2):288–93. [PubMed: 11169836]
4. Chou I-J, Tench CR, Gowland P, Jaspan T, Dineen RA, Evangelou N, Abdel-Fahim R, Whitehouse WP, Constantinescu CS. Subjective discomfort in children receiving 3 T MRI and experienced adults' perspective on children's tolerability of 7 T: a cross-sectional questionnaire survey. BMJ open. 2014; doi: 10.1136/bmjopen-2014-006094
5. Moelker A, Maas RAJJ, Pattynama PMT. Verbal Communication in MR Environments: Effect of MR System Acoustic Noise on Speech Understanding. Radiology. 2004; 232(1):107–13. [PubMed: 15220495]
6. Bandettini PA, Jesmanowicz A, Van Kylen J, Birn RM, Hyde JS. Functional MRI of brain activation induced by scanner acoustic noise. Magn Reson Med. 1998; 39(3):410–6. [PubMed: 9498597]
7. Zhang N, Zhu X-H, Chen W. Influence of gradient acoustic noise on fMRI response in the human visual cortex. Magn Reson Med. 2005; 54(2):258–63. [PubMed: 16032671]
8. Shellock FG, Ziarati M, Atkinson D, Chen DY. Determination of gradient magnetic field-induced acoustic noise associated with the use of echo planar and three-dimensional, fast spin echo techniques. J Magn Reson Imaging. 1998; 8(5):1154–7. [PubMed: 9786155]
9. Foster JR, Hall DA, Summerfield AQ, Palmer AR, Bowtell RW. Sound-level measurements and calculations of safe noise dosage during EPI at 3 T. J Magn Reson Imaging. 2000; 12(1):157–63. [PubMed: 10931575]

Author Manuscript Author Manuscript Author Manuscript Author Manuscript

10. Madio DP, Lowe IJ. Ultra-fast imaging using low flip angles and FIDs. Magn Reson Med. 1995; 34:525–529. [PubMed: 8524019]
11. Wieger M, Brunner DO, Dietrich DE, Mueller CF, Pruessmann KP. ZTE imaging in humans. Magn Reson Med. 2013; 70:328–332. [PubMed: 23776142]
12. Idiyatullin D, Corum C, Park J-Y, Garwood M. Fast and quiet MRI using a swept radiofrequency. J Magn Reson. 2006; 181(2):342–349. [PubMed: 16782371]
13. Hennel F, Girard F, Loenneker T. "Silent" MRI with soft gradient pulses. Magn Reson Med. 1999; 42(1):6–10. [PubMed: 10398943]
14. Hennel F. Fast spin echo and fast gradient echo MRI with low acoustic noise. J Magn Reson Imaging. 2001; 13(6):960–6. [PubMed: 11382960]
15. Segbers M, Rizzo Sierra CV, Duifhuis H, Hoogduin JM. Shaping and timing gradient pulses to reduce MRI acoustic noise. Magn Reson Med. 2010; 64(2):546–53. [PubMed: 20665798]
16. Heismann B, Ott M, Grodzki D. Sequence-based acoustic noise reduction of clinical MRI scans. Magn Reson Med. 2014; 73(3):1104–9. [PubMed: 24889327]
17. Alibek S, Vogel M, Sun W, Winkler D, Baker CA, Burke M, et al. Acoustic noise reduction in MRI using Silent Scan: an initial experience. Diagn Interv Radiol. 2014; 20(4):360–3. [PubMed: 24808439]
18. Corcuera-Solano I, Doshi A, Pawha PS, Gui D, Gaddipati A, Tanenbaum L. Quiet PROPELLER MRI Techniques Match the Quality of Conventional PROPELLER Brain Imaging Techniques. Am J Neuroradiol. 2015; 36(6):1124–7. [PubMed: 25678482]
19. Worters, PW., Beque, D., Peters, RD., Graziani, D., Carl, M., McKinnon, GC., Hardy, CJ. Quantitative susceptibility mapping – Comparison of silent and conventional acquisitions. Proceedings of the 24th Annual Meeting of ISMRM; Singapore. 2016; p. 4099
20. Farzaneh F, Riederer SJ, Pelc NJ. Analysis of T2 limitations and off-resonance effects on spatial resolution and artifacts in echo-planar imaging. Magn Reson Med. 1990; 14:123–39. [PubMed: 2352469]
21. Ott M, Blaimer M, Grodzki DM, Breuer FA, Roesch J, Dörfler A, et al. Acoustic-noise-optimized diffusion-weighted imaging. Magn Reson Mater Phy. 2015; 28(6):511–21.
22. Rösch J, Ott M, Heismann B, Doerfler A, Engelhorn T, Sembritzki K, et al. Quiet diffusion-weighted head scanning: Initial clinical evaluation in ischemic stroke patients at 1.5T. J Magn Reson Imaging. 2016; 44(5):1238–43. [PubMed: 26969852]
23. Schmitter S, Diesch E, Amann M, Kroll A, Moayer M, Schad LR. Silent echo-planar imaging for auditory FMRI. Magnetic Resonance Materials in Physics. 2008; 21(5):317–325.
24. Mansfield P, Chapman BL, Bowtell R, Glover P, Coxon R, Harvey PR. Active acoustic screening: reduction of noise in gradient coils by Lorentz force balancing. Magn Reson Med. 1995; 33(2): 276–281. [PubMed: 7707921]
25. Bowtell RW, Mansfield P. Quiet transverse gradient coils: Lorentz force balanced designs using geometrical similitude. Magn Reson Med. 1995; 34(3):494–497. [PubMed: 7500892]
26. Alsop DC, Connick TJ. Optimization of torque-balanced asymmetric head gradient coils. Magn Reson Med. 1996; 35:875–886. [PubMed: 8744016]
27. Edelstein WA, Hedeen RA, Mallozzi RP, El-Hamamsy SA, Ackermann RA, Havens TJ. Making MRI quieter. Magn Reson Imaging. 2002 Feb; 20(2):155–63. [PubMed: 12034336]
28. Roozen NB, Koevoets AH, Hamer den AJ. Active Vibration Control of Gradient Coils to Reduce Acoustic Noise of MRI Systems. IEEE/ASME Transactions on Mechatronics. 2008; 13(3):325–334.
29. Chronik BA, Alejski A, Rutt BK. Design and fabrication of a three-axis edge ROU head and neck gradient coil. Magn Reson Med. 2000; 44:955–963. [PubMed: 11108634]
30. Tomasi D, Xavier RF, Foerster B, Panepucci H, Tanns A, Vidoto EL. Asymmetrical Gradient Coil for Head Imaging. Magn Reson Med. 2002; 48:707. [PubMed: 12353289]
31. Yao GZ, Mechefske CK, Rutt BK. Characterization of vibration and acoustic noise in a gradient-coil insert. Magn Reson Mater Phy. 2004; 17(1):12–27.
32. Wong EC. Local head gradient coils: Window(s) of opportunity. Neuroimage. 2012; 62(2):660. [PubMed: 22245342]

Author Manuscript Author Manuscript Author Manuscript Author Manuscript

33. Mathieu, J-B., Lee, S-K., Graziani, D., et al. Development of a Dedicated Asymmetric Head-only Gradient Coil for High-Performance Brain Imaging with a High PNS Threshold. Proceedings of the 23rd Annual Meeting of ISMRM; Toronto, Canada. 2015; p. 1019
34. Lee S-K, Mathieu J-B, Graziani D, Piel J, Budesheim E, Fiveland E, Hardy CJ, Tan ET, Amm B, Foo TKF, et al. Peripheral nerve stimulation characteristics of an asymmetric head-only gradient coil compatible with a high-channel-count receiver array. Magn Reson Med. 2016; 76(6):1939–1950. [PubMed: 26628078]
35. Zhang B, Yen YF, Chronik BA, McKinnon GC, Schaefer DJ, Rutt BK. Peripheral nerve stimulation properties of head and body gradient coils of various sizes. Magn Reson Med. 2003; 50(1):50–58. [PubMed: 12815678]
36. Tan ET, Lee S-K, Weavers PT, Graziani D, Piel JE, Shu Y, Huston J, Bernstein MA, Foo TKF. High slew-rate head-only gradient for improving distortion in echo planar imaging: Preliminary experience. J Magn Reson Imaging. 2016; 44(3):653–664. [PubMed: 26921117]
37. Weavers PT, Shu Y, Tao S, Huston J, Lee S-K, Graziani D, Mathieu J-B, Trzasko JD, Foo TKF, Bernstein MA. Technical Note: Compact three-tesla magnetic resonance imager with high-performance gradients passes ACR image quality and acoustic noise tests. Medical Physics. 2016; 43(3):1259–1264. [PubMed: 26936710]
38. Boss, MA., Chenevert, TL., Waterton, JC., et al. Temperature-Controlled Isotropic Diffusion Phantom with Wide Range of Apparent Diffusion Coefficients for Multicenter Assessment of Scanner Repeatability and Reproducibility. Proceedings of the Joint Annual Meeting ISMRM-ESMRMB; Milan, Italy. 2014; p. 4505
39. Pierpaoli, C., Sarlls, J., Nevo, U., Basser, PJ., Horkay, F. Polyvinylpyrrolidone (PVP) water solutions as isotropic phantoms for diffusion MRI studies. Proceedings of the 17th Annual Meeting of ISMRM; Honolulu, Hawaii, USA. 2009; p. 1414
40. Palacios EM, Martin AJ, Boss MA, Ezekiel F, Chang YS, Yuh EL, Vassar MJ, Schnyer DM, MacDonald CL, Crawford KL, et al. Toward Precision and Reproducibility of Diffusion Tensor Imaging: A Multicenter Diffusion Phantom and Traveling Volunteer Study. Am J Neuroradiol. 2017; 38(3):537–545. [PubMed: 28007768]
41. Chu M-L, Chang H-C, Chung H-W, Truong T-K, Bashir MR, Chen N-K. POCS-based reconstruction of multiplexed sensitivity encoded MRI (POCSMUSE): A general algorithm for reducing motion-related artifacts. Magn Reson Med. 2015; 74(5):1336–1348. [PubMed: 25394325]
42. Miller KL, Pauly JM. Nonlinear phase correction for navigated diffusion imaging. Magn Reson Med. 2003; 50(2):343–353. [PubMed: 12876711]
43. Xu D, Maier JK, King KF, et al. Prospective and retrospective high order eddy current mitigation for diffusion weighted echo planar imaging. Magn Reson Med. 2013; 70:1293–305. [PubMed: 23325564]
44. Tao S, Weavers PT, Trzasko JD, Shu Y, Huston J, Lee S-K, Frigo LM, Bernstein MA. Gradient pre-emphasis to counteract first-order concomitant fields on asymmetric MRI gradient systems. Magn Reson Med. 2017; 77(6):2250–2262. [PubMed: 27373901]
45. Weavers PT, Tao S, Trzasko JD, Frigo LM, Shu Y, Frick MA, Lee SK, Bernstein MA. B0 concomitant field compensation for MRI systems employing asymmetric transverse gradient coils. Magn Reson Med. 2017 in press.
46. Tao S, Trzasko JD, Gunter JL, Weavers PT, Shu Y, Huston J, Lee SK, Tan ET, Bernstein MA. Gradient nonlinearity calibration and correction for a compact, asymmetric magnetic resonance imaging gradient system. Physics in Medicine and Biology. 2017; 62(2):N18–N31. [PubMed: 28033119]
47. Tan ET, Marinelli L, Slavens ZW, King KF, Hardy CJ. Improved correction for gradient nonlinearity effects in diffusion-weighted imaging. J Magn Reson Imaging. 2012; 38(2):448–53. [PubMed: 23172675]
48. Newitt DC, Tan ET, Wilmes LJ, Chenevert TL, Kornak J, Marinelli L, Hylton N. Gradient nonlinearity correction to improve apparent diffusion coefficient accuracy and standardization in the american college of radiology imaging network 6698 breast cancer trial. J Magn Reson Imaging. 2015; 42(4):908–19. [PubMed: 25758543]

Author Manuscript Author Manuscript Author Manuscript Author Manuscript

49. O'Halloran RL, Holmes JH, Altes TA, Salerno M, Fain SB. The effects of SNR on ADC measurements in diffusion-weighted hyperpolarized He-3 MRI. J Magn Reson. 2007; 185(1):42–49. [PubMed: 17150391]

50. Tao, AT., Shu, Y., Tan, ET., Trzasko, JD., Tao, S., Weavers, PT., Huston, J., Bernstein, MA. Improving apparent diffusion coefficient accuracy on a compact 3T MRI scanner using gradient non-linearity correction. Proceedings of the 25th Annual Meeting of ISMRM; Honolulu HI, USA. 2017. p. 1936

Author Manuscript Author Manuscript Author Manuscript Author Manuscript

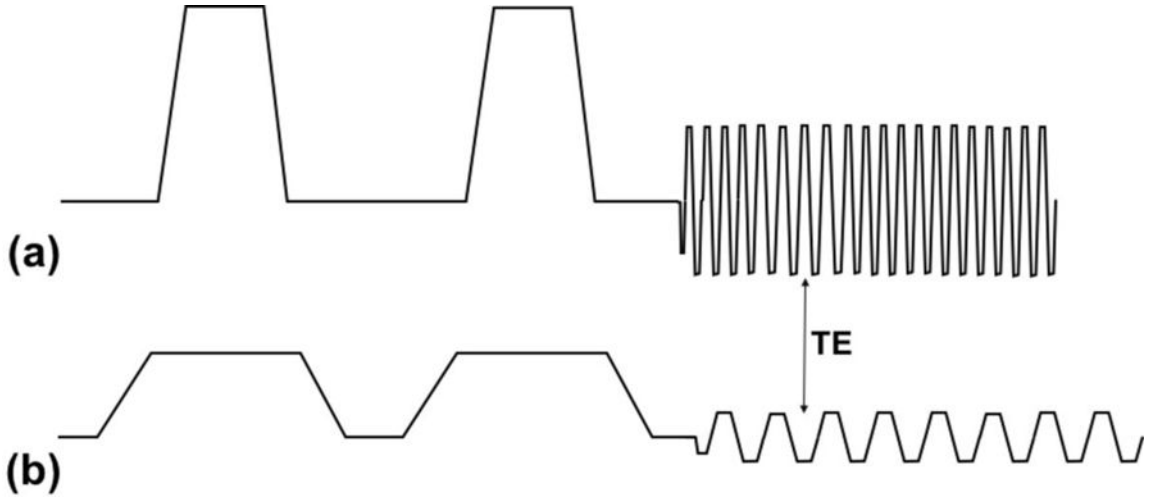

Figure 1.

Gradient waveforms used in phantom and in vivo imaging for (a) underated, single-shot DTI (diffusion amplitude = 80 mT/m, EPI amplitude = 35 mT/m, ESP = 0.33 ms) and (b) derated, single-shot DTI (diffusion amplitude = 33 mT/m, EPI amplitude = 6.4 mT/m, ESP = 2.0 ms). The echo times (TE) of both sequences were matched to the minimum TE of the derated sequence.

Author Manuscript Author Manuscript Author Manuscript Author Manuscript

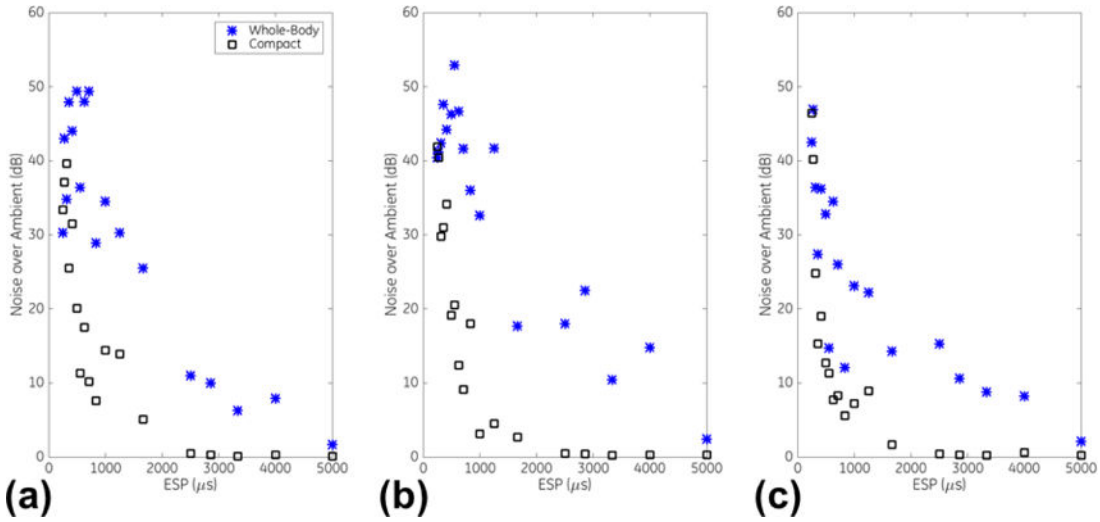

Figure 2.

Acoustic noise measurements on a whole-body 3T scanner vs. the compact 3T scanner using 10 mT/m amplitude sinusoidal gradient waveforms, of half-periodicity matching the EPI-relevant echo spacing (ESP), on the (a) X (left-right), (b) Y (anterior-posterior), and (c) Z (superior-inferior) axes.

Author Manuscript Author Manuscript Author Manuscript Author Manuscript

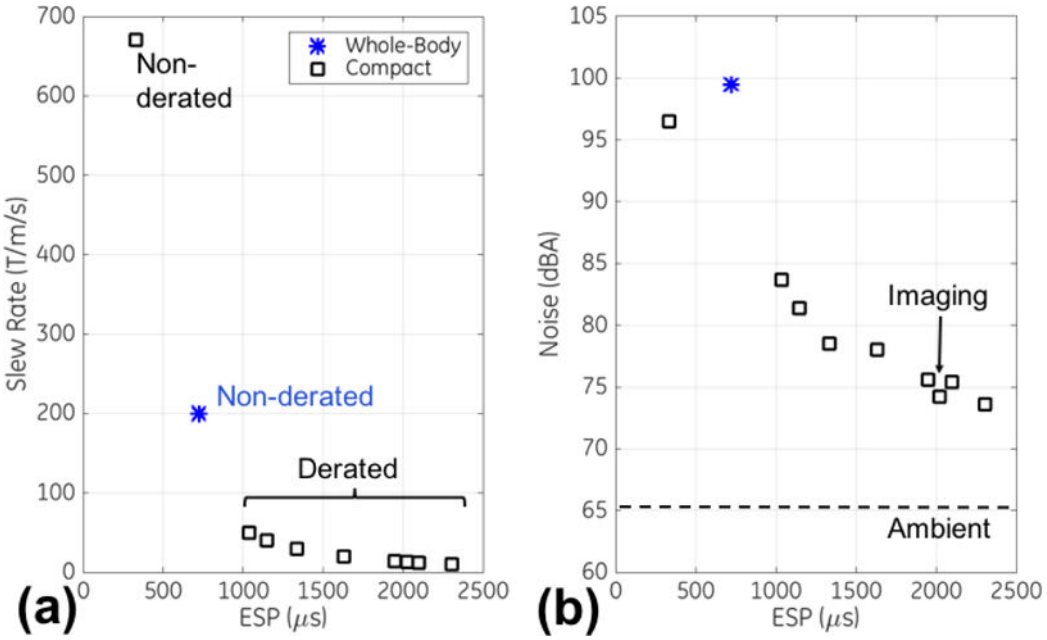

Figure 3.

Effects on EPI echo spacings (ESP) from (a) varying gradient slew rates via derating, and in turn (b) on the measured acoustic noise (in dBA). The ambient noise level measured on the compact 3T scanner (dashed) and the selected ESP for imaging (arrow) are shown.

Author Manuscript Author Manuscript Author Manuscript Author Manuscript

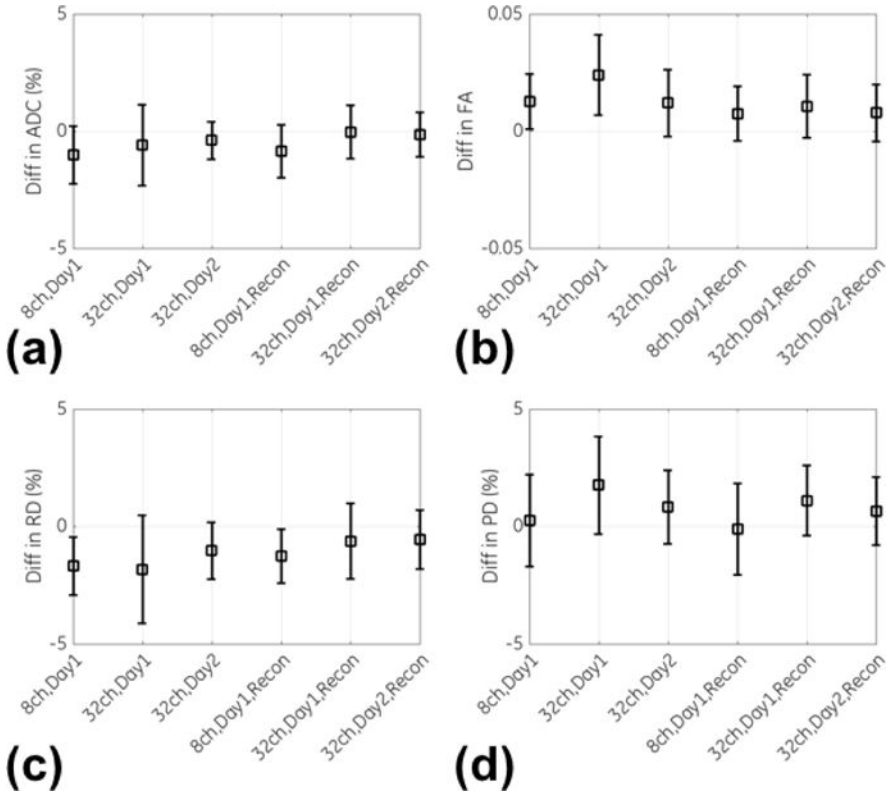

Figure 4.

Difference between diffusion metrics obtained from derated multi-shot vs. standard (non-derated) single-shot DTI in an MRS sphere phantom for various scans, with standard non-iterative reconstruction and with iterative reconstruction (indicated as “Recon”). The differences in (a) ADC, (b) FA, (c) radial diffusivity and (d) parallel diffusivity are shown, normalized as percentage differences with the exception of FA.

Author Manuscript Author Manuscript Author Manuscript Author Manuscript

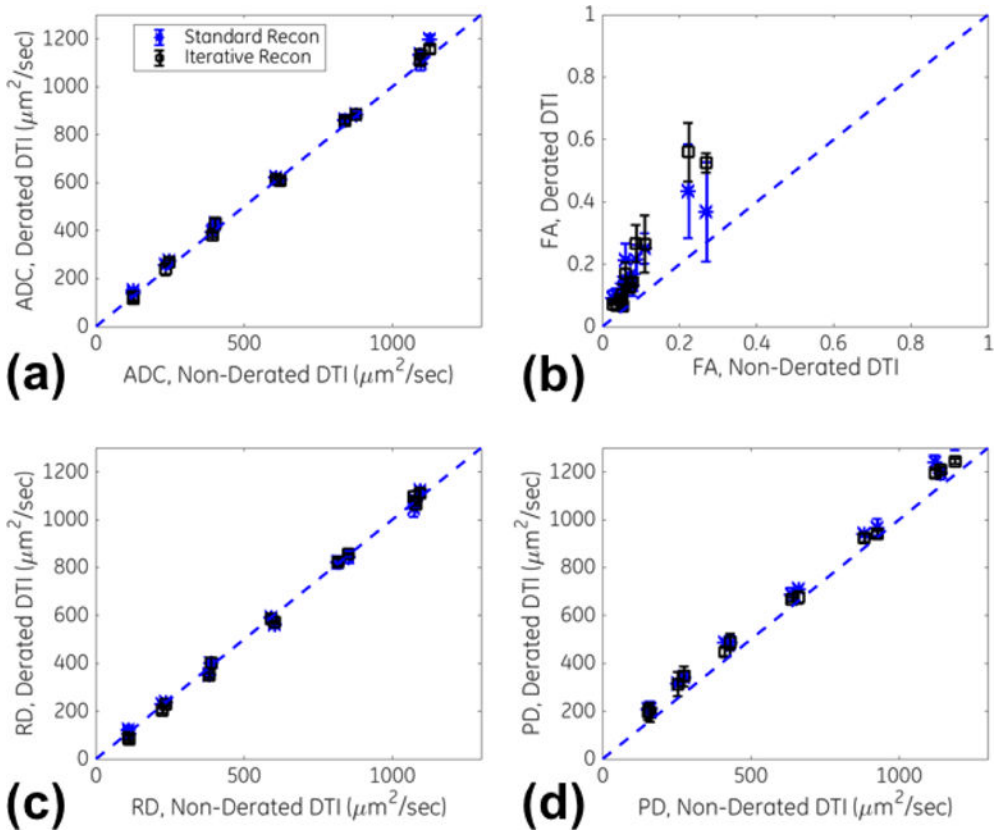

Figure 5.

Plots of diffusivity measurements in a multi-compartment, diffusion ice phantom between derated multi-shot and standard (non-derated) single-shot DTI for standard (non-iterative) reconstruction and iterative multi-shot reconstruction. Plots for (a) ADC, (b) FA, (c) radial diffusivity and (d) parallel diffusivity are shown, with the line of proportionality also shown (dashed).

Author Manuscript Author Manuscript Author Manuscript Author Manuscript

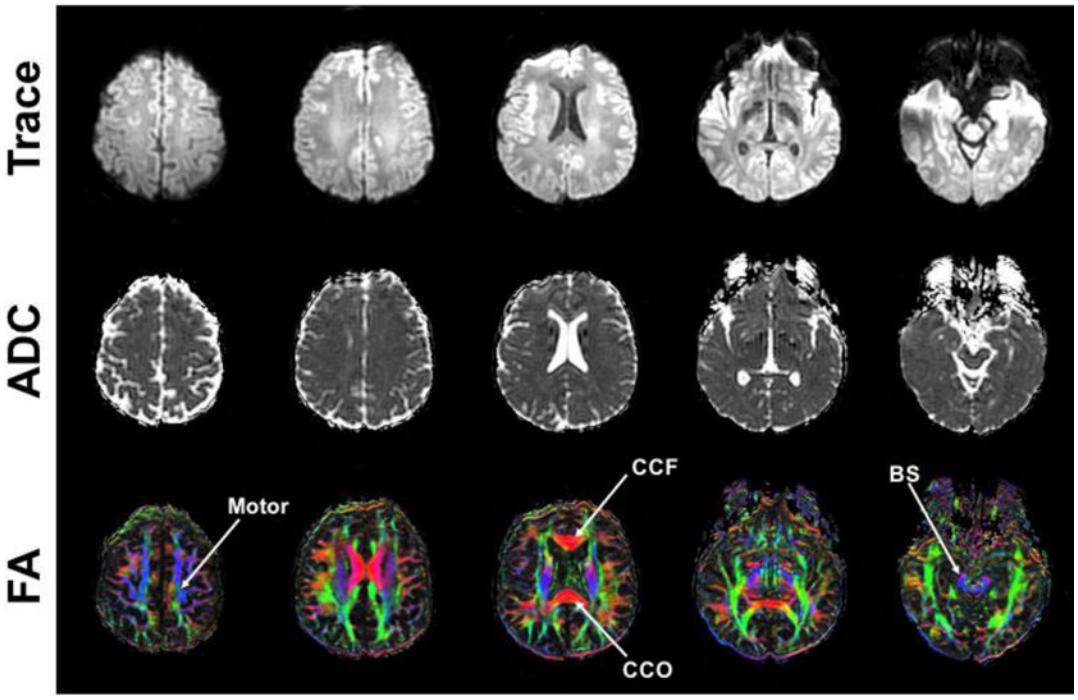

Figure 6.

Axial maps (trace diffusivity, ADC and color-encoded FA) from derated multi-shot DTI from subject #1, with selection ROI regions for motor, corpus callosum frontal/occipital (CCF/CCO), and brain stem (BS) indicated on the color-encoded FA maps.

Author Manuscript Author Manuscript Author Manuscript Author Manuscript

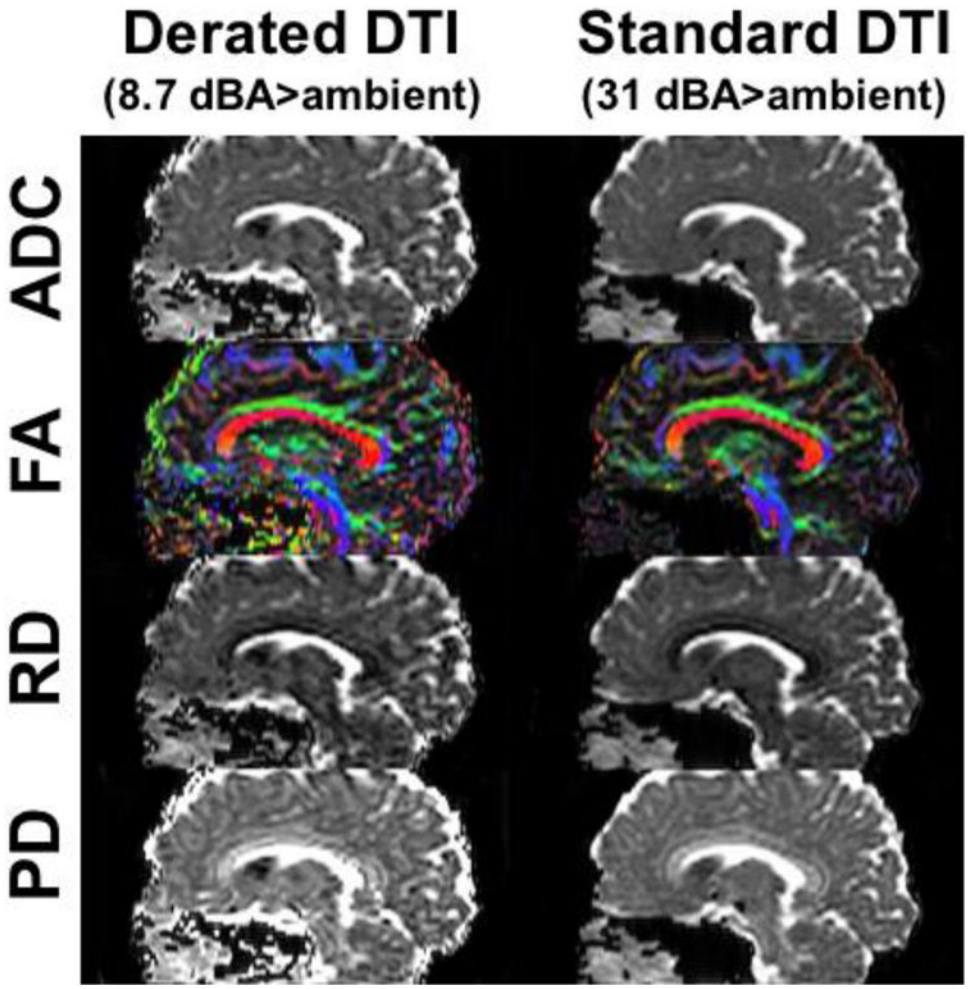

Figure 7.

Sagittal reformat of axial DTI maps from subject #5, showing comparable diffusion maps between derated multi-shot DTI and standard single-shot DTI and increased spatial distortion in the derated DTI in the phase-encoding direction (anterior-posterior, horizontal direction in this figure).

Author Manuscript Author Manuscript Author Manuscript Author Manuscript

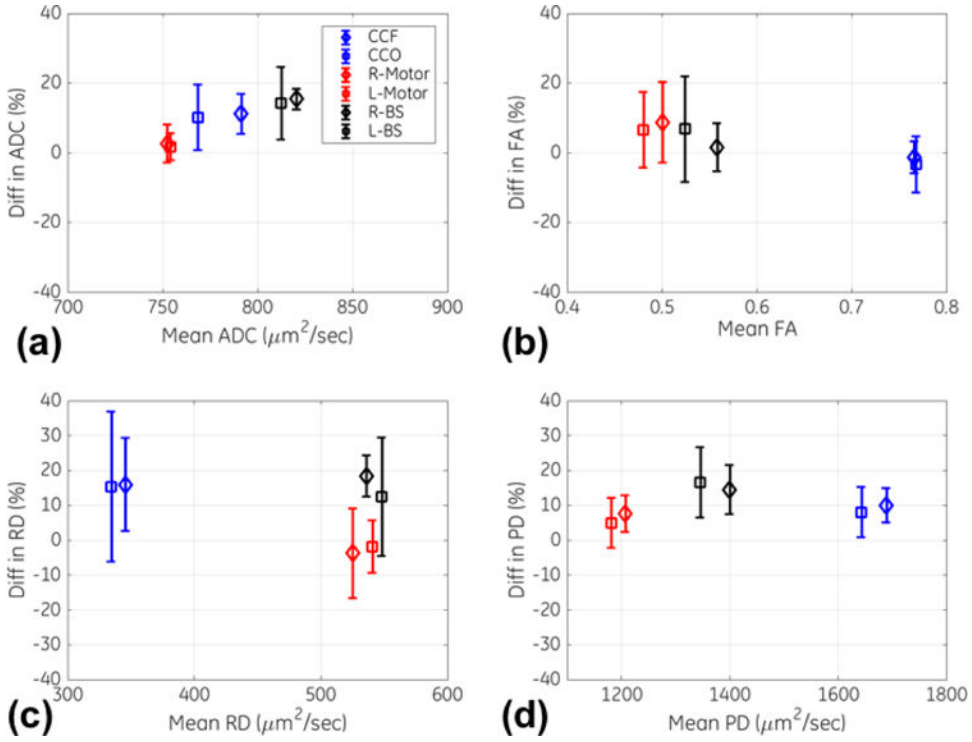

Figure 8.

Bland-Altman plots of diffusivity measurements across seven normal subjects in various brain ROI regions, with differences for the metrics obtained from derated DTI minus that from standard DTI shown. Plots are shown for (a) ADC, (b) FA, (c) RD and (d) PD. The vertical axes are normalized to show percentage differences.

Author Manuscript Author Manuscript Author Manuscript Author Manuscript

Table 1

Mean and standard deviation (SD) of ADC (in $\mu m^2/s$) from QIBA phantom, with statistically significantly different ($P<0.05$) mean ADCs different from published values [40] indicated (*).

Vial	Published Reference [40]		Standard, Non-derated Single-shot DTI		Derated Multi-shot DTI, Standard Recon		Derated Multi-shot DTI, Iterative Recon	
	Mean	SD	Mean	SD	Mean	SD	Mean	SD
0% PVP	1123	23	1105	15	1143	45	1133	22
10% PVP	850	24	859	20	874	17	871	17
20% PVP	607	19	616	10	618	12	611	10
30% PVP	408	16	398	7	413	20	406	29
40% PVP	238	11	242	7	265*	11	254	21
50% PVP	113	15	127	5	145*	8	122	16